Enhanced protection of carbon-encapsulated magnetic nickel nanoparticles through a sucrose-based synthetic strategy

ARTICLE *in* THE JOURNAL OF PHYSICAL CHEMISTRY C · APRIL 2013

Impact Factor: 4.77

8 AUTHORS, INCLUDING:

Pedro Gorria
University of Oviedo
185 PUBLICATIONS **1,744** CITATIONS
SEE PROFILE

Mariana P Proenca
University of Porto
26 PUBLICATIONS **296** CITATIONS
SEE PROFILE

Antonio B Fuertes
Spanish National Research Council
217 PUBLICATIONS **7,628** CITATIONS
SEE PROFILE

Jesus A. Blanco
University of Oviedo
313 PUBLICATIONS **1,805** CITATIONS
SEE PROFILE

THE JOURNAL OF PHYSICAL CHEMISTRY C

ARTICLE

pubs.acs.org/JPCC

Enhanced Protection of Carbon-Encapsulated Magnetic Nickel Nanoparticles through a Sucrose-Based Synthetic Strategy

Maria Paz Fernández-García,[†] Pedro Gorria,[†] Marta Sevilla,[‡] Mariana P. Proença,[§] Roberto Boada,[∥] Jesús Chaboy,[∥] Antonio B. Fuertes,[‡] and Jesús A. Blanco*[,†]

[†]Departamento de Física, Universidad de Oviedo, c/Calvo Sotelo s/n 33007, Oviedo, Spain

[‡]Instituto Nacional del Carbón (CSIC), Apartado 73, 33080, Oviedo, Spain

[§]Nanotechnology and Departamento de Física e Astronomia, Universidade do Porto, Rua do Campo Alegre, 687, 4169-007, Porto, Portugal

[∥]Instituto de Ciencia de Materiales de Aragón and Departamento de Física de la Materia Condensada, CSIC-Universidad de Zaragoza, 50009 Zaragoza, Spain

Supporting Information

ABSTRACT: We report an easy synthesis strategy for the incorporation of carbon-coated Ni nanoparticles within the pores of a highly porous carbon matrix. An advantageous feature of this process is that it is able to provide large amounts of magnetic Ni composite by means of an easy-to-follow one-pot reaction. While a typical chemical route based on a conventional pyrolysis procedure gives rise to NPs with Ni@NiO (core@shell structure), the addition of sucrose to the synthesis mixture and its subsequent transformation to carbon endows the Ni-NPs with an effective protection via the formation of a thin carbon layer around the metallic nanoparticles. This protective shell stabilizes the inserted metallic particles by preventing the aerial oxidation of Ni-NPs (i.e., NiO) and their dissolution in an aqueous acid environment. The macroscopic magnetization values of these nanocomposites (up to 6 emu/g) and their superparamagnetic behavior at room temperature allow them to be easily manipulated with conventional magnets. This makes them ideal candidates for use in applications that involve magnetic separation (i.e., heterogeneous catalysis, adsorption of contaminants in aqueous media, etc.).

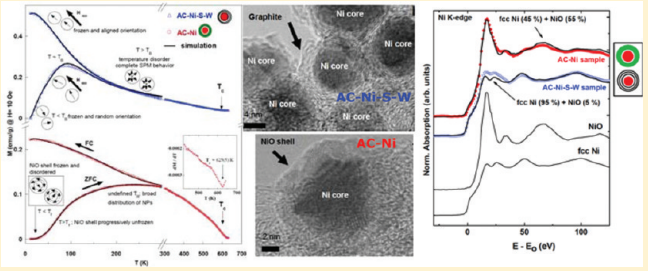

Over the past decade, the fabrication, funcionalization, manipulation, and characterization of porous materials that contain magnetic nanoparticles (NPs) have attracted great interest because they are promising candidates for many technological applications that involve magnetic separation (i.e., heterogeneous catalysis, the immobilization/separation of biomolecules, the adsorption of contaminants in aqueous media, etc.).[1−9] Indeed, these magnetic functionalities have fueled a resurgence of interest in finding ways to make their manipulation, by means of low magnetic fields (∼500 Oe), easier while ensuring that the resulting composites exhibit enough room temperature magnetization and superparamagnetic (SPM) behavior to function effectively.[10−12]

Most of these magnetic materials are made up of ferrite NPs inserted in porous carbon, silica, or polymeric matrices.[13−19] However, these ferrite NPs are in most cases unprotected, and consequently they may easily dissolve when the composite is employed in a liquid medium at pH < 2−3. A certain protection can be provided by confining the ferrite NPs inside a nonporous silica shell,[20,21] but this synthetic approach requires complex and multistep procedures. Alternatively, good protection can be provided by depositing a thin layer of carbon around these metallic NPs.[4,22−24] Nonporous metal@carbon NPs with a core@shell morphology, synthesized by means of various high-temperature pyrolysis procedures,[25−28] are being intensively investigated as contrast agents for magnetic resonance imaging (MRI) and for hyperthermia treatments due to their chemical durability and biocompatibility.[29−31]

Although the formation of protective coatings enhances the stability of the NPs and impedes clustering, the applications of such materials are still limited due to their lack of porosity. To overcome this obstacle, magnetic NPs are embedded into porous matrices of carbon.[2,4,22,25,32−37] Hence, the incorporation of magnetic metallic NPs (typically Fe, Co, and Ni) in porous carbon matrices is a first option. Another serious drawback could be the oxidation of these metallic NPs when they are exposed to air. Furthermore, magnetic metallic NPs need to be fully isolated when porous composites are employed in biomedical applications due to the toxicity of Ni and Co for live organisms.[8,38] Lu et al. have reported a multistep synthetic strategy that protects the Co NPs when they are inserted in a mesoporous carbon

Received: October 8, 2010
Revised: January 25, 2011
Published: March 15, 2011

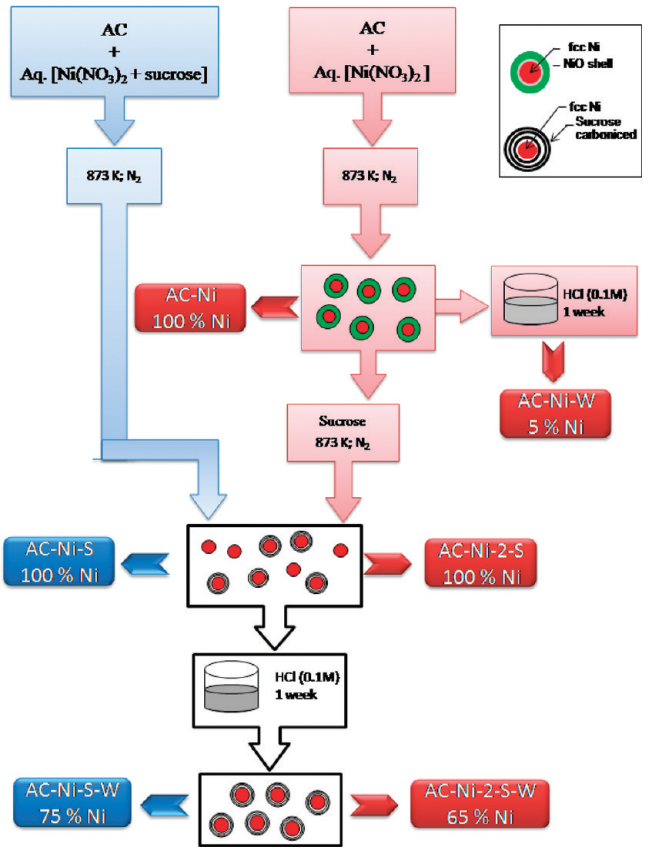

Figure 1. Illustration of the synthesis process (see details in Experimental Section).

matrix.[39] However, given the complexity of their procedure, the fabrication of magnetic porous composites with protected metallic NPs incorporated in a porous carbon matrix remains a challenge.

Accordingly, we present in this work an easy single-step reaction for the fabrication of porous magnetic composites made up of carbon coated Ni NPs embedded inside the pores of a mesoporous activated carbon (AC) matrix. The structure, morphology, and magnetic properties of these materials are investigated by means of different techniques including electron microscopy (e.g., SEM, TEM, and HRTEM), X-ray absorption spectroscopy (XANES), X-ray diffraction (XRD), and magnetometry. Moreover, we show that this composite can be fabricated with low-cost and widely available ingredients (i.e., nickel nitrate, sucrose, and a commercial activated carbon), which would make it possible to prepare the large amounts of sample necessary for applications involving magnetic separation such as those mentioned above.

RESULTS AND DISCUSSION

Formation of Ni and Ni@NiO Nanoparticles. The synthetic strategy used for the preparation of magnetic composites in this study is schematically illustrated in Figure 1. Basically, the chemical procedure is based on heat-treating (at 873 K under nitrogen atmosphere) a carbon sample impregnated first with nickel nitrate and subsequently with sucrose.[4,36] Under these conditions, the decomposition of Ni salt into NiO takes place first. Subsequently, as the temperature rises, the NiO is reduced by means of carbon, and Ni-NPs are formed. The Ni-NPs are deposited inside the restricted volume formed by the carbonaceous porous matrix. In principle, it could be expected that the size of metal NPs would be limited by the nominal pore of carbonaceous matrix, which contain pores up to 6−7 nm. However, taking into account that the porosity of the carbon matrix is made up of disordered and fully interconnected pores (see TEM image in Figure S-4 displaying this morphology), which permits the growing of metal NPs in all directions. Consequently, the size of NPs is not strictly limited by the nominal pore size of carbon matrix. A similar phenomenon has been observed in relation with the formation of large metal oxides nanostructures within of the porosity of mesostructured silica materials with interconnected pores (i.e., SBA-15).[40] By contrast, when metal oxides are synthesized within the porosity of a material with nonintercon-nected pores (e.g., MCM-41), the growth of the NPs is strictly limited by the size of the pores.[41]

When the fabrication is carried out in the absence of sucrose, the Ni-NPs formed remain unprotected, and they are rapidly oxidized into NiO at room temperature by the action of atmospheric oxygen. This process results in the formation of core@shell NPs made up of a Ni core, surrounded by a uniform-size NiO shell (Ni@NiO). It has been observed that around 95 wt % of the Ni contained in this sample (AC-Ni) is eliminated when it is treated under acid conditions (HCl 0.1 M). In contrast, when the synthesis process occurs in the presence of sucrose (AC-Ni-S sample), as much as ∼75 wt % Ni remains in the sample after the acid washing step (AC-Ni-S-W sample). This result suggests that a fraction of the carbon generated during the carbonization of the sucrose is deposited around Ni-NPs and forms a protective coat. At this point, it is worth noting that no NiO phase was detected in the AC-Ni-S-W sample even after 36 months of being stored in the lab under ambient conditions (vide infra). This clearly proves that these Ni-NPs are resistant to aerial oxidation and that they are fully protected.

We applied a similar synthetic strategy to incorporate Fe and Co NPs within the pores of the carbon with the aid of sucrose. In both cases, we found that the Fe or Co NPs generated dissolved under acid washing showing that they were unprotected.[23,33,42,43] From the present results, it seems that Ni has a special ability to associate with the carbon generated from sucrose, thus providing an effective protection against aerial oxidation. However, this issue deserves further investigation.

Structural Characteristics of Magnetic Composites. The AC matrix consists of powders at micrometer length-scale and an almost spherical morphology (see SEM images displayed in Figure S-2 in the Supporting Information). Information about the microstructure of the magnetic composites is presented in Figure 2, where several TEM and HRTEM images of the AC-Ni-S-W and AC-Ni samples are displayed. The Ni and Ni@NiO NPs are well dispersed within the carbon matrix (dark spots in Figure 2a and e), but they are not always separated as distinguishable entities in the carbonaceous matrix (gray surface in the background of the TEM images). It is well-known that the temperature of reaction kinetically governs the growth of NP and plays a crucial role in determining the size of the NPs, due to their tendency to cluster with increasing temperature (Ostwald ripening phenomenon).[44] Consequently, there is not much difference between the sizes of the Ni-NPs in the AC-Ni-S-W and AC-Ni samples because the same final temperature (873 K) was attained in their synthesis. It should also be pointed out that the deposited NPs are larger than that of the mesopores in the carbon matrix (see Experimental Section and Figure S-4 in the Supporting Information).

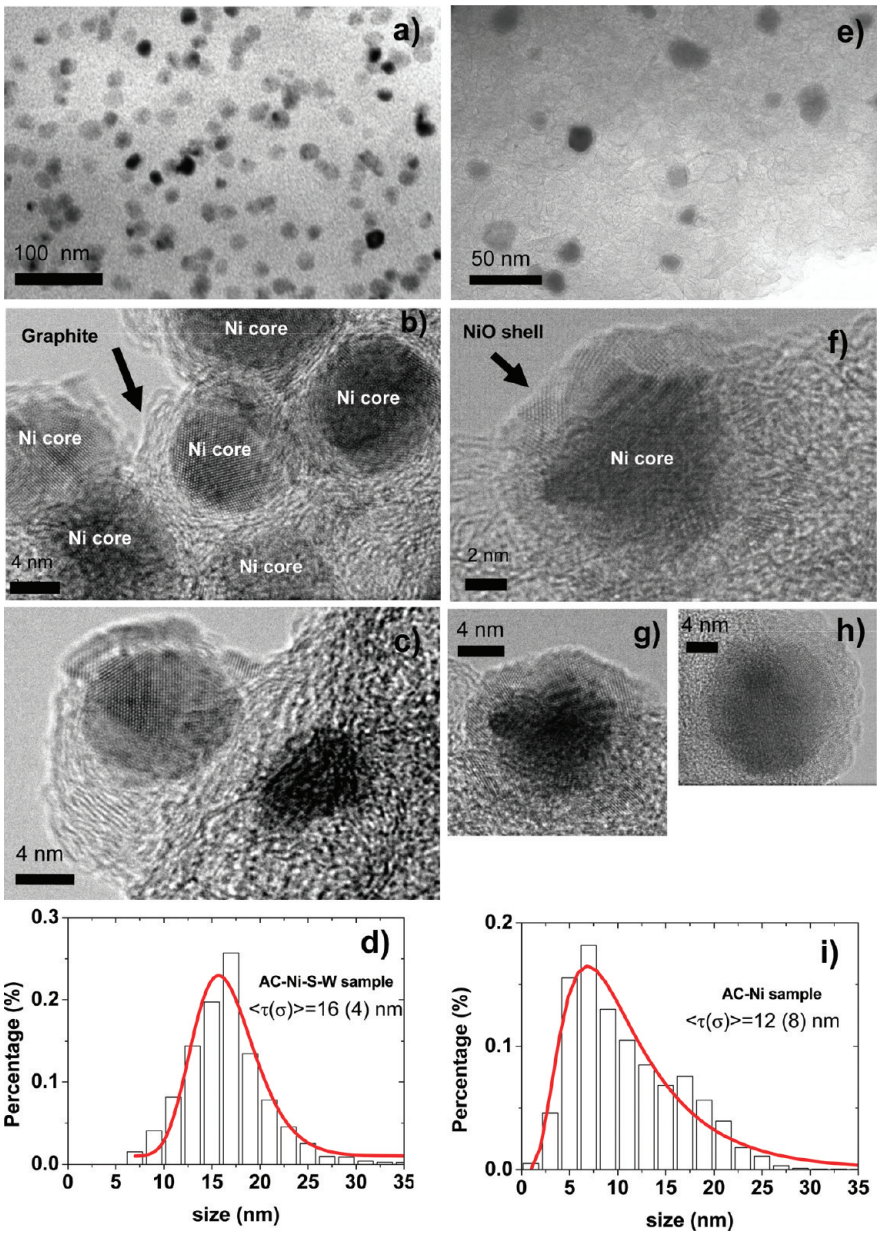

Figure 2. TEM images of the AC-Ni-S-W (a) and AC-Ni samples (e). HRTEM images of several Ni-cores fully encapsulated inside graphite shells in an AC-Ni-S-W sample are shown in (b) and (c), whereas HRTEM images of an AC-Ni composite in (f)−(h) show Ni-cores surrounded by a NiO shell in an AC-Ni sample. Histograms of the NP diameter together with fits (red solid lines) to log-normal functions of AC-Ni-S-W (d) and AC-Ni (i) samples, respectively. The mean particle sizes obtained are $\langle\tau(\sigma)\rangle$ = 16(4) nm and $\langle\tau(\sigma)\rangle$ = 12(8) nm for AC-Ni-S-W and AC-Ni samples, respectively.

The same result was also reported for iron oxide ferrite NPs deposited in an activated carbon matrix.[33] An explanation for this could be that the porosity of carbon is made up of disordered and fully interconnected pores, as commented above.

Representative HRTEM images of both samples clearly show that, whereas turbostratic carbon layers surround the Ni-NPs in the AC-Ni-S-W sample (see Figure 2b,c), no carbon coating can be detected around the Ni@NiO NPs in the AC-Ni sample (see Figure 2f−h). These results demonstrate that the carbon layer around the Ni-NPs was generated by the carbonization of sucrose. A NiO shell of ∼3 nm can be seen surrounding representative Ni-NPs in Figure 2f−h. The true nature of NiO in the Ni@NiO NPs needs to be confirmed by means of XANES.

The size distributions of the NPs were determined by measuring in several TEM images the diameters of ∼1000 isolated NPs (including the NiO-shell on the AC-Ni composite) and creating the histograms necessary to model the dimensions of the Ni-NPs [see Figure 2d and i]. These results reveal that each composite contains only one broad size distribution [ranging from 7 to 35 nm (AC-Ni-S-W sample) and from 2 to 35 nm (AC-Ni composite)], which can be satisfactorily described by a log-normal function centered at $\tau(\sigma) \approx 16(4)$ nm and $\tau(\sigma) \approx 12(8)$ nm, respectively. It is worth noting that the AC-Ni-S-W sample has a quite symmetric size distribution, while that of the AC-Ni sample is more asymmetric with a double standard deviation.

dx.doi.org/10.1021/jp109669t |J. Phys. Chem. C 2011, 115, 5294–5300

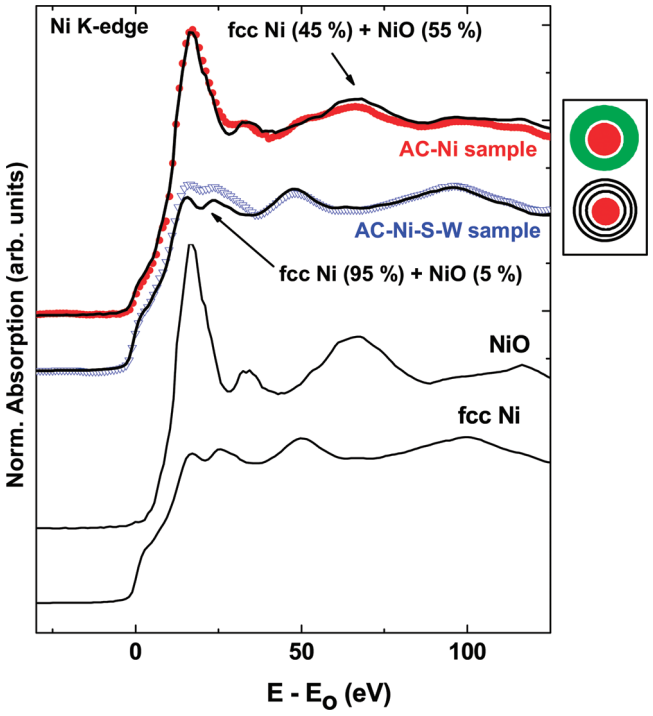

Figure 3. Ni K-edge XANES spectra for the AC-Ni (red ●) and the AC-Ni-S-W samples (blue ▽) measured at room temperature together with the simulations (black lines) for a mixture of fcc Ni and NiO. A mixture of fcc Ni (45%) and NiO (55%) was used to describe the experimental XANES of the AC-Ni composite, whereas a combination of fcc Ni (95%) and NiO (5%) was needed for the AC-Ni-S-W sample. The spectra of NiO and fcc Ni used to simulate the weighed sum (see text) are also shown at the bottom for clarity.

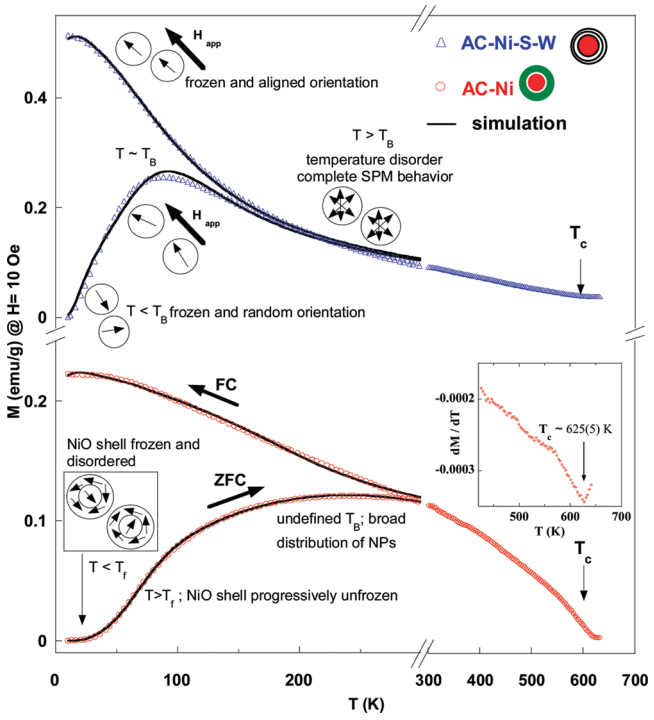

Figure 4. ZFC-FC magnetization curve of the AC-Ni-S-W (blue △) and AC-Ni (red ○) samples under an applied magnetic field $H \approx 10$ Oe. Solid lines correspond to simulations of $M_{ZFC}(T)$ and $M_{FC}(T)$ using an ideal noninteracting superparamagnetic system of NPs (see text). Characteristic temperatures such as blocking (T_B), freezing (T_f), and Curie (T_c) are schematically shown to differentiate between the several magnetic behaviors of the AC-Ni and AC-Ni-S-W samples. The magnetization units are given in emu/g (emu per gram of mass of the whole sample).

The XRD patterns for the AC-Ni-S-W and AC-Ni samples (see Figure S-3 in the Supporting Information) show that Ni crystalline NPs have a face-centered cubic (fcc) crystal structure and a cell parameter $a = 3.53$ (1) Å, close to that of bulk fcc Ni (3.52 Å).[4,36] Nevertheless, small percentages or very thin layers of metal oxides covering the metal NP cores are below the minimum coherence length required by XRD to be detected.[19] For this reason, a proper characterization of this kind of nanocomposite needs complementary techniques, such as X-ray absorption, which would provide precise and selective elemental information about the local atomic environment and the site symmetry of the tuned absorbing atomic species.[25,44]

Figure 3 shows the room temperature Ni-K edge XANES spectra of both the AC-Ni and the AC-Ni-S-W samples and compares them to those of the fcc NiO and Ni standards.

The spectral shape of the XANES is determined by the local structure around the absorbing Ni atoms. When the XANES spectra of both samples are compared, their profiles indicate that their Ni atoms are arranged differently. While the fcc Ni absorption profile is easily detected on the AC-Ni-S-W spectrum, that corresponding to the AC-Ni sample exhibits unique features characteristic of the NiO profile, suggesting the copresence of oxidized Ni with the expected metallic Ni NP cores.

Moreover, the XANES of the AC-Ni sample can be satisfactorily reproduced, in terms of shape, relative energy separation, and the intensities of their different spectral features, if a weighed mixture of fcc Ni [45 ± 5%] and NiO [55 ± 5%] is considered. In contrast, no more than 5% of NiO (which is within the range of acceptable error for this technique) is needed to properly describe the XANES spectrum of the AC-Ni-S-W sample. These results confirm that the ∼3 nm shell covering the metallic Ni cores (see Figure 2f−h) must correspond to NiO oxide. The absence of the characteristic white line of NiO in the AC-Ni-S-W sample confirms that the NiO has been almost completely eliminated during the HCl washing process, in good agreement with the HRTEM images (see Figure 2).

Magnetic Properties. We show in Figure 4 the temperature dependence of the magnetization, between 5 and 650 K, under a low applied magnetic field $H \approx 10$ Oe. The different morphology of the samples (AC-Ni-S-W is a system of single domain Ni-NPs, while AC-Ni is made up of core@shell Ni@NiO NPs) results in completely different magnetic behaviors.[45] In the case of the AC-Ni-S-W sample, the low temperature vanishing value for the magnetization measured after zero-field-cooling, $M_{ZFC} \approx 0$, points to frozen magnetic monodomains with their magnetic moments aligned in random directions (the critical diameter for Ni-NPs to behave as a magnetic monodomain is ∼60 nm).[46] On heating from $T = 5$ K the magnetization increases, and the $M_{ZFC}(T)$ curve exhibits a broad maximum centered at around 80 K. The appearance of this broad maximum is a direct consequence of the wide NP size dispersion (see Figure 2d). Hence, a more realistic picture for this system would be a distribution of blocking temperatures, T_B, rather than only one single T_B.

For temperatures above 200 K, the absence of remanence and coercivity as well as overlapping magnetization curves plotted as

dx.doi.org/10.1021/jp109669t |J. Phys. Chem. C 2011, 115, 5294–5300

a function of H/T indicate that the whole system behaves as SPM.[4,36,46,47] In the subsequent FC process, magnetic moments of the monodomains start to freeze in the direction of the externally applied magnetic field for $T < 200$ K, giving rise to a rapid increase in M_{FC}.

This description is no longer appropriate for describing the $M(T)$ response in the AC-Ni sample, because, according to the XANES and HRTEM results, the NP system exhibits a core@shell Ni@NiO morphology. First, although the mean particle size of the Ni NPs in the AC-Ni sample is smaller than those of the AC-Ni-S-W composite, the size distribution is broader and less symmetric (see Figure 2d and i). This fact explains the poorly defined maximum for the $M_{ZFC}(T)$ curve and, therefore, the lack of definition for the T_B. Second, the magnetic moments of the NiO thin shell surrounding the Ni-cores are also frozen in a magnetically disordered state (giving rise to a magnetic dead layer and/or proximity effects) of the NiO oxide below 50 K.[45,48,49] Consequently, these core@shell NPs remain blocked in a collective frozen state below a temperature known as freezing temperature, $T_f \approx 40$ K. This disordered state is responsible for the "plateau" exhibited by the $M_{ZFC}(T)$ curve below T_f (see Figure 4). For $T > T_f$, the NiO shell is unfrozen, and Ni-NPs follow the expected $M_{ZFC}(T)$ behavior with the thermal alignment of the magnetic moments in the direction of the magnetic field.

The $M(T)$ curve of the AC-Ni-S-W sample was successfully simulated by means of a procedure based on the Stoner−Wohlfarth model[50] (see solid line in Figure 4 and fitting procedure in the Supporting Information) using values of $K_{eff} = 1 \times 10^5$ erg/cm^3 and $M_s = 22$ emu/g for the effective magnetic anisotropy constant and saturation magnetization, respectively, in good agreement with the values previously reported.[49,51] On the other hand, the low-temperature frozen collective state (AC-Ni) was incorporated into the simulation taking into account the temperature dependence of K_{eff} and M_s. This allows a simple description of the gradual thermally induced unfreezing of the NiO thin shell below T_f. The simulations provide average NP-diameters of around 15 and 14 nm for the AC-Ni-S-W and AC-Ni samples, respectively, in excellent agreement with those estimated from the TEM images [16(4) and 12(8) nm, respectively] (see Figure 2d and i).

Considering the temperature dependence of magnetization above 300 K (see right-hand panel of Figure 4), it can be seen that there is a decrease in M to almost negligible values for $T > 625$ K. By estimating the Curie temperature value (T_c) of the samples from the minimum of the dM/dT dependence with temperature (see inset of Figure 4), we obtained T_c values of $\sim 625 \pm 10$ K, which is close to that of Ni-bulk[22] ($T_c \approx 627$ K). The fact that there is no enhancement of T_c indicates the absence of strains at the Ni/NiO interface and confirms the crystalline nature of both the core and the core@shell NPs.[52]

To investigate the variation of the macroscopic magnetic response in the samples subjected to different sucrose treatments, the as-prepared AC-Ni composite was made to undergo a second carbonization treatment in the presence of sucrose (AC-Ni-2-S sample, Figure 1 and the Experimental Section for further details). During this treatment two processes take place: (i) the NiO present in the AC-Ni sample is reduced to Ni by the carbon atoms, and (ii) the carbon generated from the sucrose is deposited and forms a cover around the Ni-NPs. An additional acid washing step removes the unprotected NPs. The resulting composite (AC-Ni-2-S-W) retains around 65% of the initial Ni

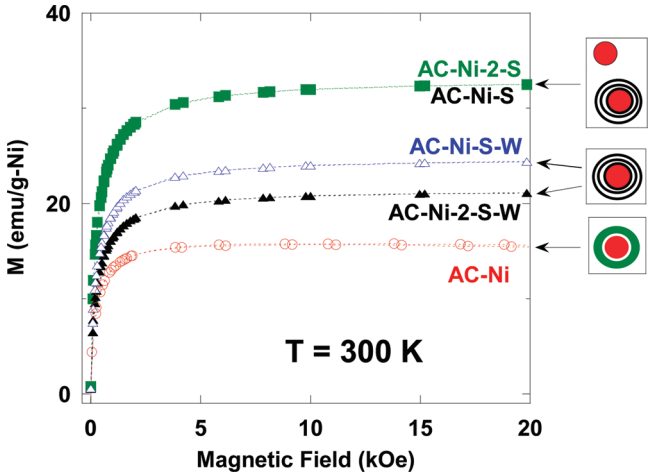

Figure 5. $M(H)$ curves near saturation recorded at room temperature for the AC-Ni-2-S and AC-Ni-S (green ■), AC-Ni-S-W (blue △), AC-Ni-2-S-W (▲), and AC-Ni (red ○) composites at 300 K. It is worth noting that the mass is normalized to the amount of nickel in the composite (see Table 1).

(see Figure 1). In Figure 5, the dependence of the magnetization with the magnetic field, $M(H)$ curves, at 300 K for all the samples investigated is displayed. The sucrose-added samples (AC-Ni-2-S and AC-Ni-S) exhibit higher magnetization values (roughly double) than that of AC-Ni due to the absence of NiO (see Figure 5). The lower value for the saturation magnetization (ca. $0.6 \cdot M_s$ of bulk-Ni) as compared to that of bulk-Ni can be attributed to the presence of random Ni magnetic moments at the NP surfaces and/or nonmagnetic Ni atoms located at the interfaces between the Ni-NPs and the carbon matrix.[34,37,48,53]

Moreover, above 200 K, the AC-Ni-2-S-W sample displays also a M versus H/T universal behavior described by a Langevin function and full reversible $M(H)$ curves indicating that this sample is in a SPM-like regime.[36] This fact is not easy to be accomplished and resembles the challenge of fabricating carbon encapsulated Ni-NPs with small dimensions.[24]

As mentioned above, the Ni-NPs are protected against acid attack by the carbonization of sucrose. After the HCl washing process, the unprotected AC-Ni-W sample becomes nonmagnetic because the Ni@NiO NPs have dissolved. Whereas the magnetization of the AC-Ni-S-W sample is only reduced by around 25% with respect to that of the AC-Ni-S composite, the magnetization of the AC-Ni-2-S sample decreases by around 33% after the acid washing (AC-Ni-2-S-W sample). Consequently, the efficiency of sucrose in protecting the Ni-NPs is confirmed. This one-pot synthetic method (aqueous solution containing sucrose and nickel nitrate) simplifies the chemical procedure and, at the same time, provides an enhanced magnetic response. Finally, it is worth noting that magnetic measurements performed on the samples stored at room temperature and in contact with air for 36 months did not reveal differences either in magnetic behavior or in saturation magnetization values.

■ CONCLUSIONS

In summary, we have successfully implemented a simple one-step procedure for the synthesis of porous magnetic composites made up of nickel nanoparticles inserted within the pores of an activated carbon. An important property of these composites is

Table 1. Sample Codes, Synthesis Conditions, and Characteristics of Magnetic Composites[a]

sample code	synthesis conditions	Ni, wt %	S_{BET}, $m^2\ g^{-1}$	V_P, $cm^3\ g^{-1}$	M_s (emu/g) at 300 K
AC-Ni	composite prepared in the absence of sucrose	10	1770	1.1	1.5
AC-Ni-W	AC-Ni sample washed with HCl 0.1 M	0.5			~0
AC-Ni-2-S	AC-Ni sample impregnated with sucrose and carbonized	10	1160	0.73	3.5
AC-Ni-2-S-W	AC-Ni-2-S sample washed with HCl 0.1 M	6.5			1.5
AC-Ni-S	composite prepared in the presence of sucrose	16	1290	0.77	5.6
AC-Ni-S-W	AC-Ni-S sample washed with HCl 0.1 M	12	1300	0.76	3.2

[a] The magnetization units are given in emu/g (emu per gram of mass of the whole sample).

that the deposited nickel nanoparticles are coated with carbon turbostratic layers that protect them against acid corrosion and aerial oxidation. This protection is attributed to the fact that the sucrose introduced in the synthesis mixture is carbonized during the pyrolysis process. A certain fraction of the formed carbonaceous residue is then deposited around the generated Ni nanoparticles thanks to the special ability of nickel to associate with the carbon generated by the sucrose. The macroscopic saturation magnetization values (~6 emu/g) together with the absence of magnetic hysteresis at room temperature make these materials easy to manipulate magnetically. Thus, these nanostructured powders are candidates for use in technological applications as separable magnetic adsorbents. This is because carbons are extremely difficult to separate from a solution, making it necessary to use complex centrifugation or filtration procedures. However, the ability of these mesoporous activated carbon matrices to incorporate protected Ni nanoparticles together with their biocompatibility and chemical stability provide novel and unique opportunities for using them in applied fields, for example, as catalyst supports, as adsorbents, and in biomedical engineering, etc. In addition, from a fundamental point of view, the possibility of tailoring the morphology of the Ni@NiO core@shell paves the way for the study of Ni magnetism at nanoscale.

EXPERIMENTAL SECTION

Preparation of the Magnetic Composites. A commercial activated carbon (AC) was employed as carbonaceous matrix for the deposition of nickel nanoparticles. The AC material, which was supplied by Osaka Gas (Japan), has a large Brunauer−Emmett−Teller (BET) surface area of 2350 $m^2\ g^{-1}$, a high pore volume of 1.47 $cm^3\ g^{-1}$, and a porosity made up of mesopores of up 6−7 nm diameter and centered at around 2.5 nm. The synthetic method is based on pyrolysis taking place within the restricted volume formed by the AC porosity. As in a typical fabrication, 1 g of AC was impregnated up to incipient wetness with a solution formed by nickel nitrate (0.7 g) and eventually sucrose (0.6 g) in 1 mL of water (see Figure 1). The impregnated sample was dried and subsequently heat-treated under N_2 up to 873 K and kept at this temperature for 3 h. Finally, the sample was cooled under nitrogen to room temperature and then passivated with a small stream of air to stabilize it. The Ni content of this sample was determined by thermogravimetric analysis (TGA). The synthesis conditions, sample codes, and main characteristics of the prepared materials are listed in Table 1.

Characterization Methods. SEM images were recorded on a SEM JEOL JSM-6100 microscope to be able to study the morphology of the porous carbon matrix and the powdered samples. TEM and HRTEM images were obtained using JEOL2000-EXII and JEM2100-JEOL microscopes (180 kV), respectively, on samples prepared by depositing a small amount of powder in ethanol and then by depositing several drops of this solution on carbon films which were placed on copper grids. Room temperature X-ray powder diffraction patterns were collected on a SIEMENS D5000 diffractometer operating at 40 kV and 20 mA, using Cu Kα radiation (λ = 1.5418 Å).

The room temperature Ni K-edge XANES spectra were recorded in transmission mode, using the BM25A (Spline) beamline at ESRF. Ni metal foil spectra were also recorded simultaneously to calibrate the energy. For the measurements, homogeneous layers of the powdered samples were prepared by spreading the powder over an adhesive tape. The thickness and homogeneity of the samples were optimized to obtain the best signal-to-noise ratio. The absorption spectra were analyzed according to standard procedures, and the spectra were normalized to the absorption coefficient averaged at high energy to eliminate the dependence of absorption on the sample thickness.

The temperature and magnetic field dependences of magnetization, $M(T,H)$, and hysteresis loops, $M(H)$, were measured using a Quantum Design PPMS-14T magnetometer with the vibrating-sample (VSM) option. First, the sample was cooled in a zero field (ZFC) from 300 to 10 K. Next, the magnetic applied field $H \approx 10$ Oe was applied and kept constant. The magnetization, M_{ZFC} and M_{FC}, values were measured at fixed temperatures (ΔT = 2 K) between 10 and 300 K and from 300 to 10 K, respectively. The magnetic field was estimated considering a standard paramagnetic material Gd_2O_3 to quantify the residual or remanent field. The $M(T)$ curves between 300 and 650 K were measured using a commercial Oxford Instruments 1.2 T resistive VSM magnetometer equipped with a furnace.

ASSOCIATED CONTENT

Supporting Information. N_2 sorption isotherms and pore size distributions (inset) of the AC-Ni-S-W and AC-Ni samples. SEM image at micrometer length scale of the AC powder. X-ray diffraction patterns of the AC-Ni-S-W and AC-Ni samples. TEM image of the porosity of the activated carbon matrix made up of disordered and fully interconnected pores of 6−7 nm. Procedure to describe the fitting of the $M(T)$ curves in the ZFC-FC regime. This material is available free of charge via the Internet at http://pubs.acs.org.

AUTHOR INFORMATION

Corresponding Author
*E-mail: jabr@uniovi.es.

■ ACKNOWLEDGMENT

Financial support from FEDER and the Spanish MICINN (grant nos. MAT2008-00407 and MAT2008-06542-C04) is acknowledged. M.P.F.-G. and R.B. thank MICINN for the award of FPI grants cofinanced by the European Social Fund. M.P.P is thankful to FCT for doctoral grant SFRH/BD/43440/2008. We are grateful to ESRF and CRG-SPline for allocating beam-time. We thank Imanol de Pedro (Univ. Cantabria) and David Martínez Blanco (SCT's Univ. Oviedo) for providing assistance with the magnetic measurements. We also thank Carlos Álvarez Villa (SCT's Univ. Oviedo) and Lidia Fernández (Univ. Cantabria) for the TEM and HRTEM images, respectively.

■ REFERENCES

(1) Doyle, P. S.; Bibette, J.; Bancaud, A.; Viovy, J. L. *Science* **2002**, *295*, 2237.
(2) Oliveira, L. C. A.; Rios, R.; Fabris, J. D.; Garg, V.; Sapag, K.; Lago, R. M. *Carbon* **2002**, *40*, 2177–2183.
(3) Lee, I. S.; Lee, N.; Park, J.; Kim, B. H.; Yi, Y. W.; Kim, T.; Kim, T. K.; Lee, I. H.; Paik, S. R.; Hyeon, T. *J. Am. Chem. Soc.* **2006**, *128*, 10658–10659.
(4) Gorria, P.; Sevilla, M.; Blanco, J. A.; Fuertes, A. B. *Carbon* **2006**, *44*, 1954–1957.
(5) Gu, H. W.; Xu, K. M.; Xu, C. J.; Xu, B. *Chem. Commun.* **2006**, *9*, 941–949.
(6) Bao, J.; Chen, W.; Liu, T. T.; Zhu, Y. L.; Jin, P. Y.; Wang, L. Y.; Liu, J. F.; Wei, Y. G.; Li, Y. D. *ACS Nano* **2007**, *1*, 293–298.
(7) Park, H. Y.; Schadt, M. J.; Wang, L.; Lim, I. I. S.; Njoki, P. N.; Kim, S. H.; Jang, M. Y.; Luo, J.; Zhong, C. J. *Langmuir* **2007**, *23*, 9050–9056.
(8) Pankhurst, Q. A.; Thanh, N. K. T.; Jones, S. K.; Dobson, J. *J. Phys. D.: Appl. Phys.* **2009**, *42*, 224001.
(9) Sanchez-Iglesias, A.; Grzelczak, M.; Rodriguez-Gonzalez, B.; Guardia-Giros, P.; Pastoriza-Santos, I.; Perez-Juste, J.; Prato, M.; Liz-Marzan, L. M. *ACS Nano* **2009**, *3*, 3184–3190.
(10) Yavuz, C. T.; Mayo, J. T.; Yu, W. W.; Prakash, A.; Falkner, J. C.; Yean, S.; Cong, L. L.; Shipley, H. J.; Kan, A.; Tomson, M.; Natelson, D.; Colvin, V. L. *Science* **2006**, *314*, 964–967.
(11) Wang, Z.; Liu, X.; Lv, M.; Meng, J. *Mater. Lett.* **2010**, *64*, 1219–1221.
(12) Dan, L.; Wey Yang, T.; Gooding, J. J.; Cordelia, S.; Rose, A. *Adv. Funct. Mater.* **2010**, *20*, 1767–1777.
(13) Lu, A. H.; Li, W. C.; Kiefer, A.; Schmidt, W.; Bill, E.; Fink, G.; Schuth, F. *J. Am. Chem. Soc.* **2004**, *126*, 8616–8617.
(14) Lee, J.; Lee, D.; Oh, E.; Kim, J.; Kim, Y. P.; Jin, S.; Kim, H. S.; Hwang, Y.; Kwak, J. H.; Park, J. G.; Shin, C. H.; Hyeon, T. *Angew. Chem., Int. Ed.* **2005**, *44*, 7427–7432.
(15) Fuertes, A. B.; Tartaj, P. *Small* **2007**, *3*, 275–279.
(16) Fuertes, A. B.; Sevilla, M.; Alvarez, S.; Valdes-Solis, T.; Tartaj, P. *Adv. Funct. Mater.* **2007**, *17*, 2321–2327.
(17) Pettigrew, K. A.; Long, J. W.; Carpenter, E. E.; Baker, C. C.; Lytle, J. C.; Chervin, C. N.; Logan, M. S.; Stroud, R. M.; Rolison, D. R. *ACS Nano* **2008**, *2*, 784–790.
(18) Valdes-Solis, T.; Rebolledo, A. F.; Sevilla, M.; Valle-Vigon, P.; Bomati-Miguel, O.; Fuertes, A. B.; Tartaj, P. *Chem. Mater.* **2009**, *21*, 1806–1814.
(19) Fernandez-García, M. P.; Gorria, P.; Blanco, J. A.; Fuertes, A. B.; Sevilla, M.; Boada, R.; Chaboy, J.; Schmool, D.; Greneche, J. M. *Phys. Rev. B* **2010**, *81*, 094418.
(20) Zhao, W.; Gu, J.; Zhang, L.; Chen, H.; Shi, J. *J. Am. Chem. Soc.* **2005**, *127*, 8916–8917.
(21) Deng, Y.; Qi, D.; Deng, C.; Zhang, X.; Zhao, D. *J. Am. Chem. Soc.* **2008**, *130*, 28.
(22) Dravid, V. P.; Host, J. J.; Teng, M. H.; Hwang, B. E. J.; Johnson, D. L.; Mason, T. O.; Weertman, J. R. *Nature* **1995**, *374*, 602.
(23) Fernández, M. P.; Schmool, D. S.; Silva, A. S.; Sevilla, M.; Fuertes, A. B.; Gorria, P.; Blanco, J. A. *J. Magn. Magn. Mater.* **2010**, *322*, 1300–1303.
(24) Huang, Y. a.; Xu, Z.; Yang, Y.; Tang, T.; Huang, R.; Shen, J. *J. Phys. Chem. C* **2009**, *113*, 6533–6538.
(25) Rojas, T. C.; Sayagues, M. J.; Caballero, A.; Koltypin, Y.; Gedanken, A.; Ponsonnet, L.; Vacher, B.; Martin, J. M.; Fernandez, A. *J. Mater. Chem.* **2000**, *10*, 715–721.
(26) Liu, B. H.; Ding, J.; Zhong, Z. Y.; Dong, Z. L.; White, T.; Lin, J. Y. *Chem. Phys. Lett.* **2002**, *358*, 96–102.
(27) Geng, J. F.; Jefferson, D. A.; Johnson, B. F. G. *Chem. Commun.* **2004**, 2442–2443.
(28) Fernandez, M. P.; Schmool, D. S.; Silva, A. S.; Sevilla, M.; Fuertes, A. B.; Gorria, P.; Blanco, J. A. *J. Non-Cryst. Solids* **2008**, *354*, 5219–5221.
(29) Lewinski, N.; Colvin, V.; Drezek, R. *Small* **2008**, *4*, 26–49.
(30) Smart, S. K.; Cassady, A. I.; Lu, G. Q.; Martin, D. J. *Carbon* **2006**, *44*, 1034–1047.
(31) Panessa-Warren, B. J.; et al. *J. Phys.: Condens. Matter* **2006**, *18*, S2185.
(32) Oliete, P. B.; Rojas, T. C.; Fernandez, A.; Gedanken, A.; Koltypin, Y.; Palacio, F. *Acta Mater.* **2004**, *52*, 2165–2171.
(33) Fuertes, A. B.; Tartaj, P. *Chem. Mater.* **2006**, *18*, 1675–1679.
(34) Wang, D.-W.; Li, F.; Lu, G. Q.; Cheng, H.-M. *Carbon* **2008**, *46*, 1593–1599.
(35) Sheng, Z. M.; Wang, J. N. *Carbon* **2009**, *47*, 3271–3279.
(36) Gorria, P.; Fernandez-Garcia, M. P.; Sevilla, M.; Blanco, J. A.; Fuertes, A. B. *Phys. Status Solidi RRL* **2009**, *3*, 4–6.
(37) El-Gendy, A. A.; Ibrahim, E. M. M.; Khavrus, V. O.; Krupskaya, Y.; Hampel, S.; Leonhardt, A.; Buchner, B.; Klingeler, R. *Carbon* **2009**, *47*, 2821–2828.
(38) Tartaj, P. *J. Phys. D: Appl. Phys.* **2003**, *36*, 182.
(39) Lu, A. H.; Schmidt, W.; Matoussevitch, N.; Bonnemann, H.; Spliethoff, B.; Tesche, B.; Bill, E.; Kiefer, W.; Schuth, F. *Angew. Chem., Int. Ed.* **2004**, *43*, 4303–4306.
(40) Tian, B.; Liu, X.; Yang, H.; Xie, S.; Yu, C.; Tu, B.; Zhao, D. *Adv. Mater.* **2003**, *15*, 1370–1374.
(41) Bourlinos, A. B.; Simopoulos, A.; Boukos, N.; Petridis, D. *J. Phys. Chem. B* **2001**, *105*, 7432–7437.
(42) Fernandez-García, M. P.; Gorria, P.; Sevilla, M.; Fuertes, A. B.; Boada, R.; Chaboy, J.; Aquilanti, G.; Blanco, J. A. *Phys. Chem. Chem. Phys.* **2011**, *211*, 927–932.
(43) Fernandez-García, M. P.; Gorria, P.; Sevilla, M.; Fuertes, A. B.; Greneche, J. M.; Blanco, J. A. *J. Alloys Compd.* **2011**, doi: 10.1016/j.jallcom.2010.12.206.
(44) Winnischofer, H.; Rocha, T. C. R.; Nunes, W. C.; Socolovsky, L. M.; Knobel, M.; Zanchet, D. *ACS Nano* **2008**, *2*, 1313–1319.
(45) Johnston-Peck, A. C.; Wang, J. W.; Tracy, J. B. *ACS Nano* **2009**, *3*, 1077–1084.
(46) Dormann, J. L.; Fiorani, D.; Tronc, E. *Magnetic Relaxation in Fine-Particle Systems*; John Wiley & Sons, Inc.: New York, 1997; Vol. XCVIII.
(47) Bedanta, S.; Kleemann, W. *J. Phys. D: Appl. Phys.* **2009**, *42*, 013001.
(48) Del Bianco, L.; Boscherini, F.; Fiorini, A. L.; Tamisari, M.; Spizzo, F.; Antisari, M. V.; Piscopiello, E. *Phys. Rev. B* **2008**, *77*, 094408.
(49) Nunes, W. C.; De Biasi, E.; Meneses, C. T.; Knobel, M.; Winnischofer, H.; Rocha, T. C. R.; Zanchet, D. *Appl. Phys. Lett.* **2008**, *92*, 183113.
(50) Stoner, E. C.; Wohlfarth, E. P. *IEEE Trans. Magn.* **1991**, *27*, 3475–3518.
(51) Tomita, S.; Jönsson, P. E.; Akamatsu, K.; Nawafune, H.; Takayama, H. *Phys. Rev. B* **2007**, *76*, 174432.
(52) Feygenson, M.; Kou, A.; Kreno, L. E.; Tiano, A. L.; Patete, J. M.; Zhang, F.; Kim, M. S.; Solovyov, V.; Wong, S. S.; Aronson, M. C. *Phys. Rev. B* **2010**, *81*, 014420.
(53) Jiao, J.; Seraphin, S.; Wang, X. K.; Withers, J. C. *J. Appl. Phys.* **1996**, *80*, 103–108.